Efficient computation of quasiperiodic oscillations in nonlinear systems with fast rotating parts

Schilder, F.; Rubel, J.; Starke, J.; Osinga, H.M.; Krauskopf, B.; Inagaki, M.

published in
Nonlinear Dynamics
2008

DOI (link to publisher)
10.1007/s11071-007-9242-1

document version
Publisher's PDF, also known as Version of record

Nonlinear Dyn (2008) 51:529–539
DOI 10.1007/s11071-007-9242-1

ORIGINAL ARTICLE

Efficient computation of quasiperiodic oscillations in nonlinear systems with fast rotating parts

Frank Schilder · Jan Rübel · Jens Starke · Hinke M. Osinga · Bernd Krauskopf · Mizuho Inagaki

Received: 28 April 2006 / Accepted: 5 January 2007 / Published online: 3 March 2007

Abstract We present a numerical method for the investigation of quasiperiodic oscillations in applications modeled by systems of ordinary differential equations. We focus on systems with parts that have a significant rotational speed. An important element of our approach is that it allows us to verify whether one can neglect gravitational forces after a change of coordinates into a corotating frame. Specifically, we show that this leads to a dramatic reduction of computational effort. As a practical example, we study a turbocharger model for which we give a thorough comparison of results for a model with and without the inclusion of gravitational forces.

Keywords Invariant tori · Noise · Oil-whirl · Quasiperiodic oscillation · Rotordynamics · Turbocharger · Unbalance oscillation · Vibration

F. Schilder (✉) · H. M. Osinga · B. Krauskopf
Bristol Center for Applied Nonlinear Mathematics, Department of Engineering Mathematics, University of Bristol, Queen's Building, University Walk, Bristol BS8 1TR, UK
e-mail: f.schilder@bristol.ac.uk

J. Rübel
Interdisciplinary Center for Scientific Computing (IWR) and Institute of Applied Mathematics, University of Heidelberg, Im Neuenheimer Feld 294, D-69120 Heidelberg, Germany

J. Starke
Department of Mathematics, Technical University of Denmark, Matematiktorvet, Building 303, DK-2800 Kongens Lyngby, Denmark

M. Inagaki
Toyota Central Research and Development Laboratories, Inc., Nagakute, Aichi 480-1192, Japan

1 Introduction

Rotordynamics is a discipline of mechanics that is concerned with the study of the dynamics of systems containing parts that rotate with a significant angular momentum [3]. Rotating mechanical systems are ubiquitous and examples range from the dynamics of planets, satellites, and spinning tops to machines such as turbines, compressors, pumps, helicopters, gyroscopic wheels, and computer hard drives. There has been a keen interest in rotordynamics since the first steam engines and there is an extensive literature, especially in engineering; for overviews we refer to [2, 5, 24, 27].

We present a numerical method for computing a specific type of response of nonlinear systems arising in rotordynamics and elsewhere, namely, quasiperiodic oscillations with two independent frequencies. Our method is based on computing invariant tori on which quasiperiodic oscillations take place. It is applicable to any model given in the form of a nonlinear ordinary differential equation (ODE). We demonstrate it here for a system with fast rotating parts, where we investigate the influence of the gravitational force

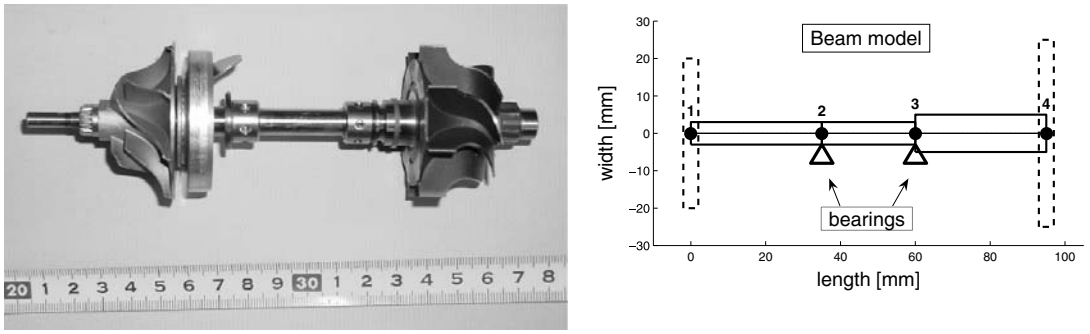

Fig. 1 The rotor of a turbocharger (a) and the simple beam model (b) with two disks at nodes 1 and 4 and oil-lubricated journal bearings at nodes 2 and 3

on the dynamics. The example under consideration is a finite-element model with oil-film forces of a symmetric rotor of a turbocharger, which is used in many modern internal combustion engines of passenger cars and heavy trucks to reduce fuel consumption and to raise the engine's power; see Fig. 1a. The turbocharger consists of a rotor shaft with a disk on either side: a turbine and an impeller. The turbine is driven by the exhaust gases. Their energy is transmitted via the rotor shaft to the impeller wheel, which compresses the inlet air into the engine cylinders for more efficient combustion. The rotor is supported by fluid film bearings and is contained inside a casing attached to the engine block.

Several mechanical eigenmodes may be excited in a turbocharger. Unavoidable manufacturing tolerances always lead to some unbalance of the rotor, which imposes a harmonic forcing of the rotor with the rotation frequency. This forcing typically leads to resonances with the first bending mode of the rotor. Furthermore, the oil-lubricated journal bearings lead to self-excited oscillations of the rotor. This instability of a rigid conical mode of the rotor is known as oil whirl [13] and has been investigated since the 1920s [19, 27]. We estimate that these modes as well as the rigid parallel modes, all of which may appear as forward and backward whirling modes, have natural frequencies in the target frequency range up to 1500 Hz; see also [10, 25]. Mathematically, the nonlinear coupling of the harmonically forced rotor and the bearings leads to complicated bifurcation behavior. For example, we find torus (Neimark–Sacker) bifurcations with subsequent quasiperiodic behavior and phase locking (entrainment); see also [1, 9, 26].

In our investigation we consider a relatively simple, but still suitable model from a hierarchy of models with an increasing number of finite elements as shown in Fig. 1b. The rotor is modeled with three Rayleigh beam elements and two rigid disks that are attached at the end nodes [18, 27]. The two inner nodes are located at the oil lubricated journal bearings and the boundary conditions are defined at these nodes by oil film forces; see Section 3 for more details. Although our model is simple it has all the essential features to capture the experimentally observed phenomena.

In some situations, it may be possible to simplify a system with fast rotating parts by neglecting the influence of the gravitational force. To this end, we introduce a corotating frame and obtain an ODE with a small time-dependent forcing term representing gravity. Due to the dominance of unbalance and oil-film forces over gravity, it seems reasonable to ignore this small forcing term for sufficiently high rotational speeds, which results in an autonomous ODE. This means that a quasiperiodic response could be approximated by a simple superposition of a periodic response of an autonomous ODE with a rotation on a circle. We demonstrate how our method may be used *a posteriori* to verify such a reduction, and to determine where the conditions for this reduction are not met, for example, when the rotational speed is too low.

2 Experiments and data analysis

Several experiments were carried out at Toyota Central R&D Laboratories for a turbocharger used in vehicle engines. The turbocharger was driven by pressurized air and operated at different rotational speeds from 7500 rpm to 101,000 rpm. The z-axis was aligned with the shaft at rest, and the horizontal (x) and vertical (y) deflections of the shaft were measured by eddy

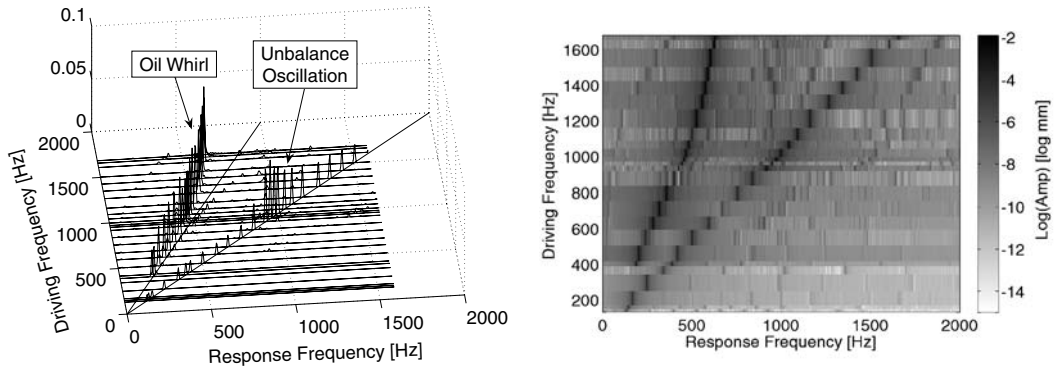

Fig. 2 Power spectrum of vibrations measured in an experiment for ramping up the driving frequency of the rotor from 130 to 1700 Hz; panel (a) shows a waterfall diagram and panel (b) a logarithmic intensity plot

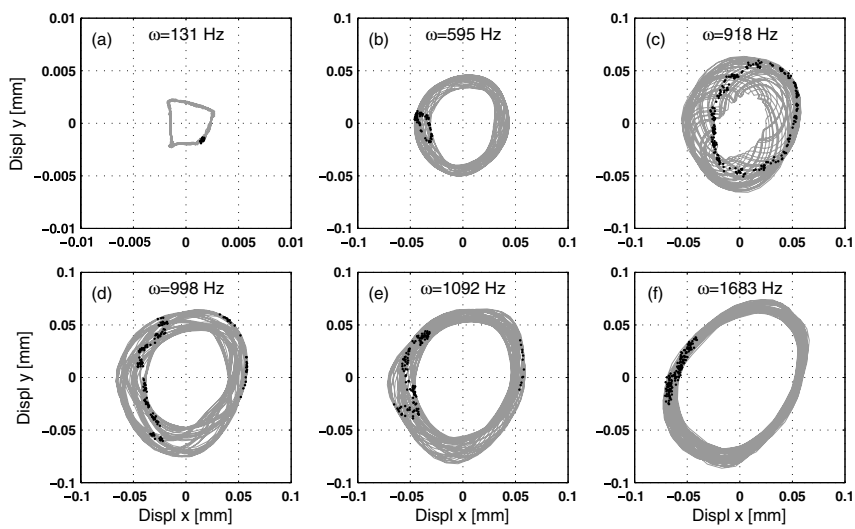

Fig. 3 Orbits of turbine dynamics (*gray*) overlaid with their Poincaré sections (*black*) measured for different rotational speeds (note the different scale for $\omega = 131$ Hz)

current sensors at both ends and in the middle of the rotor (in between the two simple journal bearings; see Fig. 1). The experimental results are shown in the frequency diagrams in Fig. 2 in two different ways. One can clearly observe the two principal vibration modes as peaks in the waterfall diagram (a) and as darker lines in the intensity plot in panel (b), which are due to unbalance and oil whirl. The harmonic part has a resonance peak at about 1000 Hz and the subharmonic part sets in at a threshold forcing frequency of about 400 Hz. The frequency of the latter vibration is slightly less than half the forcing frequency and deviates further for higher rotational speeds. The amplitude of the subharmonic part decreases in the resonance region of the harmonic part.

Figure 3 shows the increasingly complex behavior of the orbits measured at the turbine end of the shaft. For small rotational speeds (250 Hz), the orbit is periodic with a small amplitude. As the driving frequency rises above 400 Hz, a second frequency appears, which results in quasiperiodic dynamics on a torus. Such behavior is best analyzed by stroboscopic or Poincaré maps: We mark the position of the turbine every time the impeller crosses the x-axis from positive to negative values. The periodic orbit of the turbine end of the shaft that we observe for low rotational speeds corresponds to a fixed point of the stroboscopic map; see Fig. 3a. For increasing rotational speeds, the Poincaré map shows invariant circles indicating the existence of invariant tori; see Figs. 3b and c. For even higher speeds, the invariant circles show phase locking; see Figs. 3d–f.

Figure 4 shows the two mode shapes that were identified as being responsible for the two kinds of

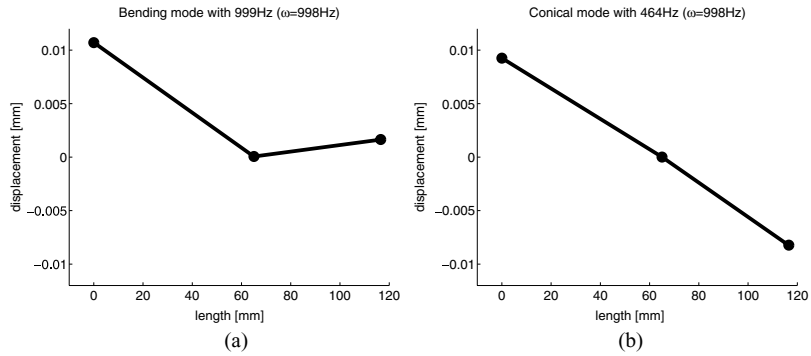

Fig. 4 The two main vibration modes at 998 Hz; bending mode (a) and conical mode (b)

vibrations observed in the experiments. The harmonic part is mainly due to a bending vibration (a), whereas the subharmonic part has a conical mode shape (b). The occurrence of the subharmonic has been observed a long time ago [19, 27]. This self-excited vibration is an oil whirl that is caused by the nonlinearity of the supporting oil film, which is included in our model. In a series of papers [13–15], Muszynska clarified the occurrence and the stability of this unwanted phenomenon. In the resonance region of the first bending mode of the shaft, the amplitude of the self-excited oil whirl drops; see Fig. 2. While several modes could become excited in principle, we found in the experiment that only the forward whirling rigid conical mode (of 464 Hz) and the forward whirling first bending mode (of 999 Hz) are actually excited.

3 Finite-element rotor model with oil-film forces

Following [27], we derived a finite beam-element model for the rotor. For the beam elements, we consider rotating Rayleigh beams that take into account bending, rotary inertia due to bending, and gyroscopic effects, but neglect shear deformation and torsion. The rotor is split into three parts of constant diameter; see Fig. 1b. The z-axis is the horizontal axis and each element $w_i(z) = [u_i(z), v_i(z)]$ is described by lateral displacements u_i and v_i in the x- and y-directions and the inclinations $\phi_{x,i} = \partial u_i/\partial z$ and $\phi_{y,i} = \partial v_i/\partial z$ at its end-nodes. We collect all displacements and inclinations in the vector $q_i = (u_i, v_i, \phi_{x,i}, \phi_{y,i})$ and use standard cubic C^1 element functions as shape functions; see, for example, [18].

Two rigid disk elements representing the turbine and compressor wheels are attached to the shaft in nodes 1 and 4 and their motion is completely described by the coordinates of these nodes. Using standard variational techniques [12, 18] and setting $x = (q_1, q_2, q_3, q_4)$, we obtain the equation of motion

$$\begin{aligned}\hat{L}x &:= M\ddot{x} + (C + \omega G)\dot{x} + Kx \\ &= F_{\mathrm{b}}(x, \dot{x}) + F_{\mathrm{g}} + \omega^2 A(\omega t) F_{\mathrm{unb}} \end{aligned} \tag{1}$$

for the shaft. Here, $\hat{L}$ is a second-order differential operator with symmetric mass, damping, and stiffness matrices M, C, and K, respectively, and skew-symmetric gyroscopic matrix G. Furthermore, ω is the angular velocity of the rotor and F_{g} is the gravitational force. Nodes 2 and 3 are placed at the locations of the two oil-lubricated journal bearings and can move freely. The forces F_b exerted by the bearings are computed by integrating the pressure distribution in the bearings over the journal surface. To keep the model simple, we use the well-known short bearing approximation of Reynolds' equation with Gümbel boundary conditions for the pressure distribution [2, 24]. The oscillating forces due to unbalance are modeled by the term $\omega^2 A(\omega t) F_{\mathrm{unb}}$, where F_{unb} is a constant vector and $A(\omega t)$ is a 16×16 block-diagonal rotation matrix with eight 2×2 diagonal blocks of the form

$$B(\omega t) = \begin{pmatrix} \cos\,\omega t & -\sin\,\omega t \\ \sin\,\omega t & \cos\,\omega t \end{pmatrix}.$$

Note that $A(\omega t)^{-1} = A(\omega t)^{\mathrm{T}}$ and $\|A(\omega t)\|_2 = 1$.

A drawback of system (1) is that the absolute value of the time-dependent unbalance forces $\omega^2 A(\omega t) F_{\mathrm{unb}}$ is large since this term grows quadratically with the driving frequency. As an important part of our approach, we transform Equation (1) into a corotating frame; see also textbooks such as [2, 5, 18, 24, 27]. For the model coordinates $q_i = (u_i, v_i, \phi_{x,i}, \phi_{y,i})$ in the fixed frame

as defined earlier, let p_i be the corresponding coordinates in a frame that is rotating about the z-axis with rotational speed ω. That is, we apply the transformation

$$q_i = \begin{pmatrix} B(\omega t) & 0 \\ 0 & B(\omega t) \end{pmatrix} p_i,$$

which leads to the equation of motion

$$\tilde{L}y = \widetilde{F}_{\mathrm{b}}(y, \dot{y}) + A(\omega t)^{\mathrm{T}} F_{\mathrm{g}} + \omega^2 F_{\mathrm{unb}}, \tag{2}$$

where $y = (p_1, p_2, p_3, p_4)$ is the collection of coordinates in the corotating frame. The time-dependent term $A(\omega t)^{\mathrm{T}} F_{\mathrm{g}}$ is a $2\pi/\omega$-periodic forcing due to gravity. Both Equations (1) and (2) are 16-dimensional second-order ODEs with right-hand sides that explicitly depend on time. For computational purposes, we transform these equations into equivalent 32-dimensional first-order ODEs.

The advantage of Equation (2) over Equation (1) is that for higher rotational speeds the gravitational force is small compared with the bearing and unbalance forces. This raises the question whether or not the influence of gravity can be neglected under certain circumstances. If we omit the gravitational forcing term, then Equation (2) no longer depends explicitly on time. This greatly simplifies the numerical treatment of quasiperiodic vibrations of the turbocharger model, because the dynamics on the underlying torus can then be decomposed into two independent oscillations. One oscillation is just the forcing ωt taken modulo 2π, and the other is a periodic solution with frequency ω_2 of the now autonomous Equation (2). The computation of periodic solutions is a matter of seconds to minutes, but the computation of tori requires minutes to hours, or even days. The main reason for this increase in computation time is that a torus is a two-dimensional surface, whereas a periodic solution is a one-dimensional curve. While the computation time depends only little on the dimension of the system, it increases dramatically with the dimension of the object of interest.

4 Computation of quasiperiodic oscillations

A popular approach for the numerical investigation of response solutions is simulation, that is, solving a sequence of initial value problems for an ODE model over a range of parameters of interest. In combination with tools for classifying solutions, one can compute so-called brute-force bifurcation diagrams. This technique is usually very time consuming, even though one can easily distribute the workload by subdividing the parameter ranges.

An alternative is to use numerical continuation and bifurcation methods. These techniques not only provide efficient means of computing certain types of solutions, but also allow one to detect and classify bifurcations; see, for example, [8, 11, 16, 17, 23] for background information on bifurcation theory. For the computation of equilibria and periodic solutions, one can use well-established software packages, for example, AUTO [4] that provide methods for detecting pitchfork, transcritical, period-doubling, and Neimark–Sacker bifurcations. Furthermore, loci of such bifurcations can be computed in a two-parameter plane.

The computation of invariant tori is currently an active area of research; we refer to the introduction of [20] for a recent overview. We apply below a recently developed method for the numerical continuation of quasiperiodic tori.

4.1 Numerical method

A vibration with two or more (but finitely many) incommensurate frequencies is a quasiperiodic solution of an ODE. A quasiperiodic solution never repeats and densely covers an invariant torus in phase space; see the experimental data in Figs. 3b and c. In [21], we presented a method, which we also apply here, for the computation of quasiperiodic solutions with two incommensurate frequencies; see also [6, 22]. The basic idea of this method is to compute an invariant circle of the period-$2\pi/\omega_1$ stroboscopic map, which is the intersection of the torus with the plane $t = 0$. Here, $\omega_1 = \omega$ is the forcing frequency and we interpret time as an angular variable modulo the forcing period. By construction, the invariant circle has rotation number $\varrho = \omega_2/\omega_1$, where ω_2 is the additional response frequency of the occurring vibration. An invariant circle with rotation number ϱ is a solution of the so-called invariance equation

$$u(\theta + 2\pi\varrho) = g(u(\theta)), \tag{3}$$

where u is a 2π-periodic function and g is the period-$2\pi/\omega_1$ stroboscopic map of (2). We approximate the

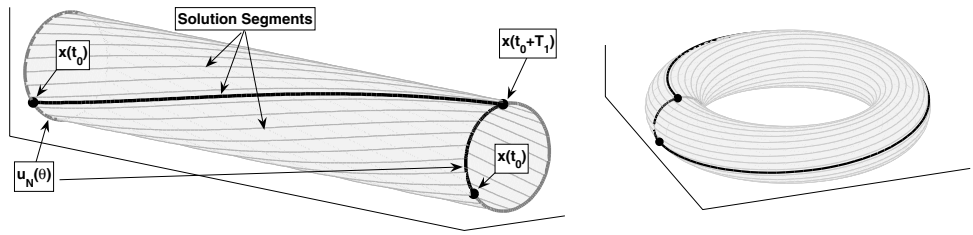

Fig. 5 Illustration of the invariance equation (3). The solution curve starting at the point $x(t_0)$ crosses the invariant circle again in the point $x(t_0 + T_1)$ after one period (a). In angular coordinates on the invariant circle, we have $x(t_0 + T_1) = u(\theta_0 + 2\pi\varrho)$. If we identify the circles at both ends of the tube, we obtain a torus (b)

invariant circle u with a Fourier polynomial of the form

$$u_N(\theta) = c_1 + \sum_{k=1}^{N} c_{2k} \sin k\theta + c_{2k+1} \cos k\theta \tag{4}$$

and compute the real coefficient vectors $c_1, \ldots, c_{2N+1}$ by collocation. The stroboscopic map g is computed with the second-order fully implicit midpoint rule as the solution of a two-point boundary value problem; see [21] and Fig. 5 for more details.

We construct seed solutions for our subsequent continuations of tori with the method of homotopy. To this end, we introduce an artificial parameter $\lambda \in [0, 1]$ as an amplitude of the gravitational forcing:

$$\tilde{L}y = \widetilde{F}_{\mathrm{b}}(y, \dot{y}) + \lambda A(\omega t)^{\mathrm{T}} F_{\mathrm{g}} + \omega^2 F_{\mathrm{unb}}. \tag{5}$$

We refer to the case $\lambda = 0$ as the *zero-gravity system* and the case $\lambda = 1$ as the *Earth-gravity system*. The principle of homotopy is to compute a torus for $\lambda = 0$ and try to follow this torus as λ is slowly increased up to $\lambda = 1$. For $\lambda = 0$, Equation (5) becomes autonomous and we can construct an invariant torus directly from a Fourier approximation of the form (4) of a periodic solution with frequency ω_2. This can be seen from the definition of the period-$2\pi/\omega_1$ stroboscopic map of the $T_2 = 2\pi/\omega_2$-periodic solution $x(t) = u_N(\omega_2 t) = u_N(\theta)$, where u_N is our Fourier polynomial of order N with the scaling $\omega_2 t = \theta$. Then, $x(t + T_1) = g(x(t)) = g(u_N(\theta))$ by definition, and we also have

$$\begin{aligned} x(t + T_1) &= x\left(\frac{\theta}{\omega_2} + \frac{2\pi}{\omega_1}\right) \\ &= x\left(\frac{1}{\omega_2}\left[\theta + 2\pi\frac{\omega_2}{\omega_1}\right]\right) = u_N\left(\theta + 2\pi\varrho\right). \end{aligned}$$

Finally, a solution segment connecting a starting point $x(t_0) = u_N(\theta_0)$ with its endpoint $x(t_0 + T_1)$ is given by $u_N(\theta)$, where $(\theta - \theta_0) \in [0, 2\pi\varrho]$; see Fig. 5.

For the system under consideration it turns out that the zero-gravity tori are such accurate approximations to the Earth-gravity tori that the latter can be computed in just one homotopy step; compare panels (b) and (c) of Fig. 6 where we computed a series of tori for varying radial bearing clearance c_r and driving frequency ω. The fact that the zero-gravity tori are almost identical to the Earth-gravity tori is a first indication that neglecting gravity is a valid and powerful simplification of the model equation.

Recall that the reason for performing such a simplification whenever feasible is the fact that the numerical analysis of invariant tori (for $\lambda = 1$) is a much harder problem than the analysis of periodic solutions (for $\lambda = 0$). Furthermore, the dependence of periodic solutions on system parameters can be studied by changing the parameters individually. This is no longer true for quasiperiodic tori, because a quasiperiodic vibration with two incommensurate frequencies can be changed into a phase-locked state by arbitrarily small changes in any parameter [7, 11, 23]. Therefore, one simultaneously needs to adjust a second free parameter to "follow" solutions with a fixed frequency ratio. Thus, loci of quasiperiodic tori are curves in a two-parameter plane: for example, note the slight shift in some of the positions of Earth-gravity tori in Fig. 6a with respect to the seed solutions. The union of these curves covers a set of large measure [7, 11, 23]. In other words, there is a non-zero probability to observe quasiperiodic behavior in physical systems.

We emphasize at this point that, according to the above construction, the computation of periodic solutions for $\lambda = 0$ is equivalent to a computation of invariant tori for $\lambda = 0$. Our claim is that these tori are

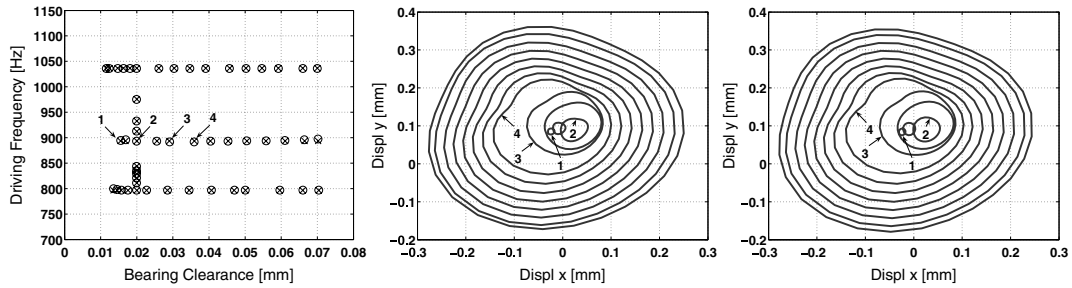

Fig. 6 Positions of the seed solutions (label ×) and corresponding earth-gravity tori (label ○) in the (c_r, ω) plane (a). The invariant circles for Earth gravity (b) and the corresponding periodic solutions for zero gravity (c) for the starting positions along the row near $\omega \approx 894$ Hz. The tori at the labeled positions are shown in Fig. 7

good approximations of the tori for $\lambda = 1$ for certain parameters. Our method allows one to identify such parameter regions where neglecting gravity is a sound assumption. In these regions, one can obtain the response behavior of the turbocharger model by studying the periodic solutions of the autonomous ODE (5) with $\lambda = 0$.

4.2 Computational results

We focus here on computations that demonstrate the performance of our numerical technique, and how it can be used for testing the validity of the zero-gravity assumption. We sweep the two-parameter plane of radial bearing clearance c_r and forcing frequency ω with a large number of curves of Earth-gravity tori with fixed rotation number to obtain a picture as complete as possible. We then compare these results with the respective computations of periodic solutions for the zero-gravity approximation. Toward the end of this section, we give a physical interpretation of the results. All our computations were performed on Equation (5) in corotating coordinates. Note that, due to the shift in frequencies, the rotation numbers ϱ_f in the fixed frame and ϱ_r in the corotating frame systems are related via $\varrho_f = |\varrho_r - 1|$. In the results shown later, we find $\varrho_r \leq 1$, thus $\varrho_f = 1 - \varrho_r$.

First, we compute a Fourier approximation of the periodic solution of the zero-gravity system for $\omega = 1000$ Hz and $c_r = 0.02$ mm. This is done by simulation and a subsequent Fourier transformation with $N = 15$ Fourier modes in Equation (4). We then perform a continuation of the periodic solution with respect to the forcing frequency and select the solutions that are shown as the column of crosses for $c_r = 0.02$ in Fig. 6a in the frequency window $\omega \in [700\,\text{Hz}, 1200\,\text{Hz}]$, which is a principal range of operation for the turbocharger. In a second run, we compute the start solutions marked by the three rows of crosses for frequencies $\omega = 797$ Hz, 894 Hz, and 1037 Hz in the range $c_r \in [0.01\,\text{mm}, 0.08\,\text{mm}]$, which represents the design margin of the device.

As explained in the previous section, we construct initial approximations of tori in the Earth-gravity system from these periodic solutions. We computed these tori with $N = 15$ Fourier modes and $M = 100$ Gauß collocation points and keep this mesh size fixed for all subsequent computations. In the homotopy step, we keep the radial bearing clearance c_r fixed and take the forcing frequency ω as a secondary free parameter. The obtained starting positions of tori are marked with circles in Fig. 6a. The idea is that, with this distribution of starting solutions, the loci of tori with fixed rotation numbers cover the (c_r, ω)-plane densely enough to allow meaningful conclusions. Note that the starting positions virtually coincide with the seed positions. The differences in the forcing frequencies mean that tori with a certain rotation number are observed for slightly different rotational speeds in the two systems. In other words, the response frequencies differ somewhat.

A first comparison of the two types of solutions is given in panels (b) and (c) of Fig. 6. Both graphs illustrate the change of the invariant circle in the stroboscopic map as the bearing clearance is increased and the forcing frequency is kept (approximately) constant. The two sets of circles are clearly very similar. The full tori for the starting positions labeled 1–4 are shown in Fig. 7 together with a plot of the displacements at node 1. Even though our finite beam-element model with oil-film forces is quite coarse, the numerical

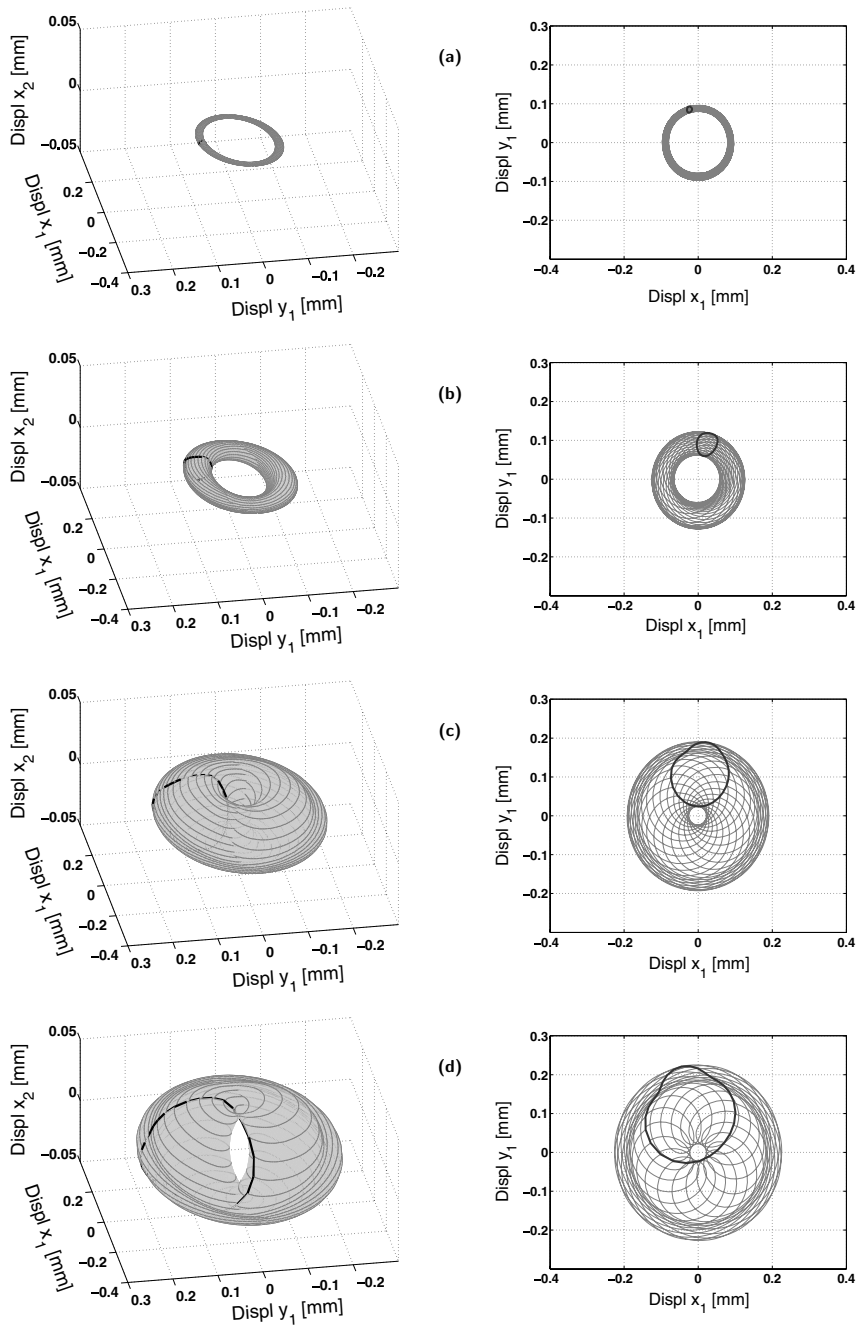

Fig. 7 The left-hand column of (a)–(d) shows starting tori with labels 1, 2, 3 and 4, respectively, along the row $\omega = 894$ Hz in Fig. 6a. The corresponding x- and y-displacements at the first FEM-node are shown in the right-hand column. The dark closed curve is the invariant circle of the period-$2\pi/\omega_1$ stroboscopic map

results resemble the qualitative features of the measured orbits; compare Fig. 7b with Fig. 3c. Note that the Poincaré sections are defined differently in these figures.

A comparison of the two sets of resulting two-parameter curves is shown in Fig. 8 with loci of tori with fixed rotation number in panel (a) and loci of periodic solutions with fixed frequency ratio in panel (b). The color bar indicates the rotation numbers (shifted back to fixed-frame frequencies) that are associated with these curves. The second response frequency ω_2 is the product of this shifted rotation number with the driving frequency shown on the vertical axis. These curves match very well: Only in a band around 900 Hz, there are some

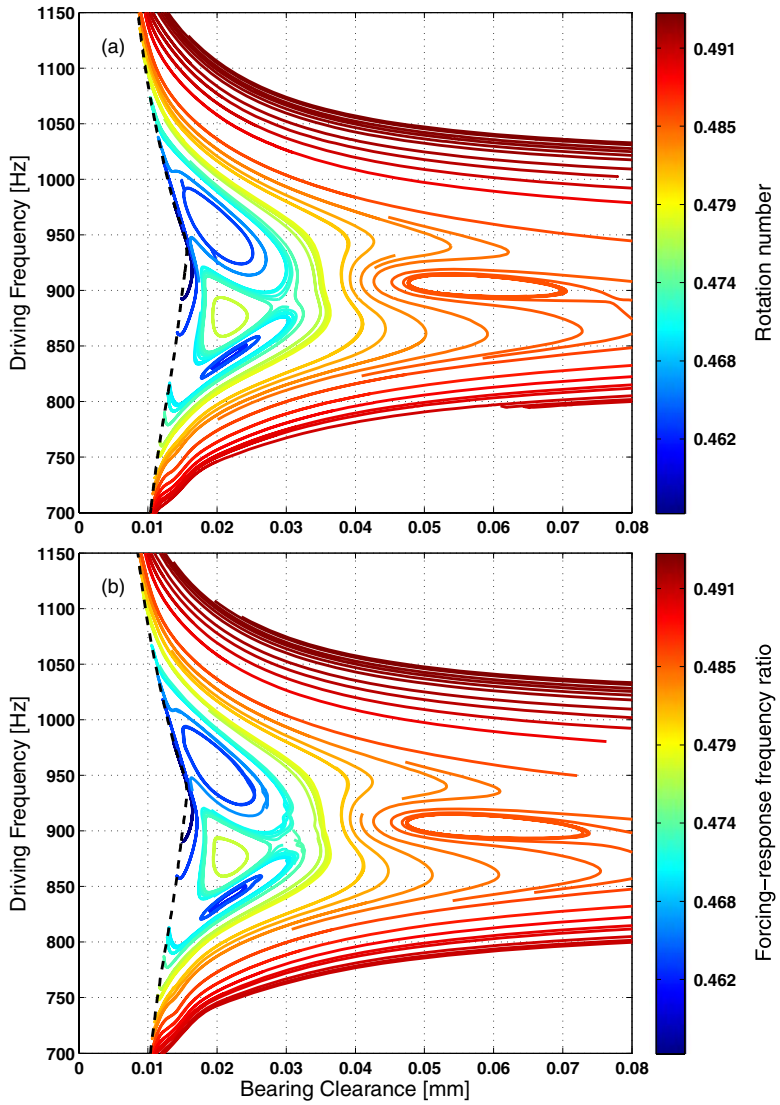

Fig. 8 Curves of quasiperiodic tori with fixed rotation number of the Earth-gravity system (a) and curves of periodic solutions with fixed frequency ratio of the zero-gravity system (b). The diagram gives an overview of the second response frequency as a function of the bearing clearance and the forcing frequency. The color bar indicates the rotation number or frequency ratio associated with each curve, which was shifted back to fixed-frame frequencies for easier interpretation. The dashed curve in panel (a) is the locus of Neimark–Sacker bifurcations, and the dashed curve in panel (b) is the locus of Hopf bifurcations. The second frequency is suppressed to the left of these curves, that is, there are no tori for bearing clearances smaller than ≈0.01 mm

visible differences, but they are small. At a first glance, we observe that in the region covered ω_2 is approximately half the driving frequency, in accordance with the experimental data; see Fig. 2. If we keep the bearing clearance fixed at 0.02 mm, as used in the current design of the turbocharger, and increase the driving frequency, then the rotation number decreases initially, stays almost constant for $\omega \in [830\,\text{Hz}, 970\,\text{Hz}]$, and then starts to increase. This behavior occurs in the same region as the "bending" of the oil-whirl response frequency away from the straight line $\omega_2 = 0.5\omega$ in Fig. 2.

Figure 8 also shows two bifurcation curves (dashed), namely, a locus of Neimark–Sacker bifurcations (a) and the corresponding locus of Hopf bifurcations (b). Again, these curves match very well. For small bearing clearance, to the left of the Neimark-Sacker curve, the response is periodic and has the same frequency as the forcing; this corresponds to an equilibrium solution for the zero-gravity system. If we cross this curve from left to right the quasiperiodic response considered earlier is born and its amplitude grows rapidly as the bearing clearance is further increased; see Figs. 6b and 7. This behavior is also accurately captured in the zero-gravity system as is illustrated with panels (b) and (c) of Fig. 6, where periodic solutions are compared with invariant circles of tori along the line $\omega = 894\,\text{Hz}$. These results indicate that for the range of forcing frequencies considered here, a reduction of the bearing

clearance could dramatically reduce the amplitude of the quasiperiodic vibration or even suppress the second frequency completely.

Figure 8a shows a total of 51 curves of tori and along each curve we computed 200 tori (this is the reason why some curves end in the middle of the figure). The computation of the tori took approximately 4 weeks on an Intel Xeon CPU 2.66 GHz, that is, the average time to compute one torus is about 4 min. The computation of the corresponding curves of periodic solutions in panel (b) with the same number of solutions along each curve was completed within 24 h, that is, the computation of one periodic solution takes about 9 s. Hence, the transition to the zero-gravity system results in a large gain in performance, possibly at the expense of some accuracy. However, as our computations show, the qualitative behavior of the two systems virtually coincides for the investigated parameters, and one might ask whether the introduced approximation error is at all significant. Our results clearly suggest that one could perform an analysis of periodic solutions of the zero-gravity system and look at the Earth-gravity system only for reference and verification.

5 Conclusions

In this paper, we demonstrated the efficient computation of invariant tori for a simple finite beam-element turbocharger model with oil-film forces. In our study, the bearing clearance and the driving frequency were the main parameters. From a physical point of view, a large bearing clearance leads to the undamping of the conical mode via oil-film forces. Our investigation verified that one can neglect gravitational forces for higher rotational speeds. We showed that this leads to a dramatic reduction of computational effort if the model is formulated in corotating coordinates. The reason is that invariant tori of the Earth-gravity system are then well approximated by tori constructed from periodic solutions of the zero-gravity system. The computation of periodic solutions is a much simpler task and there are well-established and highly efficient methods at hand that could be applied to substantially more detailed models of a turbocharger, or other machinery with fast rotating parts.

If gravity or other static loads cannot be considered to be small perturbations, then one must compute invariant tori in the Earth-gravity system. Such a computation is far more challenging and there are only few methods available. The recently developed method [21] used here works well for moderately large systems and shows a typical tradeoff: the computation of tori requires more memory than long-term simulation, since all mesh points and a large sparse matrix need to be stored simultaneously. On the other hand, it is faster, more accurate, and provides more detailed information about the dynamics. Furthermore, it allows to compute unstable tori and, thus, the direct analysis of hysteresis effects.

The techniques used here for the turbocharger model are also applicable more widely. In particular, for other systems with fast rotating parts it may be possible to neglect the influence of gravity and obtain the powerful reduction as discussed in this paper. The value of invariant torus computations is that they allow one to verify the validity of this type of model reduction. In this case, a bifurcation diagram showing the qualitative behavior of the response solutions can be obtained with the computation of periodic solutions alone.

Acknowledgements This work was supported by EPSRC Grant GR/R72020/01, Toyota CRDL, and the University of Heidelberg.

References

1. Bonello, P., Brennan, M.J., Holmes, R.: An investigation into the non-linear dynamics of an unbalanced flexible rotor running in an unsupported squeeze film damper bearing. Proc. Inst. Mech. Eng. Part C: J. Mech. Eng. Sci. **217**, 955–971 (2003)
2. Childs, D.: Turbomachinery Rotordynamics. Wiley, New York (1993)
3. Crandall, S.H.: Rotordynamics. In Kliemann, W., et al. (eds.) Nonlinear Dynamics and Stochastic Mechanics. Dedicated to Prof. S. T. Ariaratnam on the Occasion of his Sixtieth Birthday, CRC Mathematical Modelling Series, pp. 3–44. CRC, Boca Raton, FL (1995)
4. Doedel, E.J., Champneys, A.R., Fairgrieve, T.F., Kuznetsov, Yu.A., Sandstede, B., Wang, X.: Auto97: Continuation and Bifurcation Software for Ordinary Differential Equations (with HomCont). Technical report, Concordia University (1997), available at: URL: *http://cmvl.cs.concordia.ca/auto/*
5. Gasch, R., Nordmann, R., Pfützner, H.: Rotordynamik, 2nd edn. Springer, Berlin Heidelberg New York (2002)
6. Ge, T., Leung, A.Y.T.: Construction of invariant torus using Toeplitz Jacobian matrices/fast Fourier transform approach. Nonlinear Dyn. **15**(3), 283–305 (1998)
7. Glazier, J.A., Libchaber, A.: Quasi-periodicity and dynamical systems: an experimentalist's view. IEEE Trans. Circuits Syst. **35**(7), 790–809 (1988)

8. Hayashi, Ch.: Nonlinear Oscillations in Physical Systems, McGraw-Hill Electrical and Electronic Engineering Series. McGraw-Hill, New York (1964)
9. Holt, C., San Andres, L., Sahay, S., Tang, P., La Rue, G., Gjika, K.: Test response and nonlinear analysis of a turbocharger supported on floating ring bearings. ASME J. Vib. Acoust. **127**, 107–115 (2005)
10. Kijimoto, Sh., Matsuda, K., Kanemitsu, Y.: Stability-optimized clearance configuration of fluid-film journal bearings. In: Proceedings of ASME International Design Engineering Technical Conference & Computers and Information in Engineering Conference, 24–28 September, DETC2005-84671, Long Beach, CA (2005)
11. Kuznetsov, Yu.A.: Elements of Applied Bifurcation Theory, Vol. 112, Applied Mathematical Sciences, 3rd edn. Springer-Verlag, New York (2004)
12. Meirovitch, L.: Elements of Vibration Analysis, 2nd edn. Wiley, New York (1986)
13. Muszynska, A.: Whirl and whip – rotor/bearing stability problems. J. Sound Vib. **110**(3), 443–462 (1986)
14. Muszynska, A.: Tracking the mystery of oil whirl. Sound Vib. **21**(2), 8–12 (1987)
15. Muszynska, A.: Stability of whirl and whip in rotor/bearing systems. J. Sound Vib. **127**(1), 49–64 (1988)
16. Nayfeh, A.H.: Nonlinear Interactions. Wiley-Interscience, New York (2000)
17. Nayfeh, A.H., Balachandran, B.: Applied Nonlinear Dynamics. Wiley, New York (1995)
18. Nelson, H.D., McVaugh, J.M.: The dynamics of rotor-bearing systems using finite elements. ASME J. Eng. Ind. **98**(2), 593–600 (1976)
19. Newkirk, E.L., Taylor, H.D.: Shaft whirling due to oil action in journal bearings. Gen. Electr. Rev. **28**(7), 559–568 (1925)
20. Schilder, F., Osinga, H.M., Vogt, W.: Continuation of quasi-periodic invariant tori. SIAM J. Appl. Dyn. Syst. **4**(3), 459–488 (2005) (electronic)
21. Schilder, F., Peckham, B.B.: Computing Arnol′d tongue scenarios. J. Comput. Phys. **220**(2), 932–951 (2007)
22. Schilder, F., Vogt, W., Schreiber, S., Osinga, H.M.: Fourier methods for quasi-periodic oscillations. Int. J. Numer. Methods Eng. **67**(5), 629–671 (2006)
23. Strogatz, S.H.: Nonlinear Dynamics and Chaos: With Applications to Physics, Biology, Chemistry, and Engineering. Cambridge University Press, Perseus Publishing, New York (2000)
24. Vance, J.M.: Rotordynamics of Turbomachinery. Wiley, New York (1988)
25. Wagner, B.B., Ginsberg, J.H.: The effect of bearing properties on the eigenvalues of a rotordynamic system. In: Proceedings of ASME International Design Engineering Technical Conference & Computers and Information in Engineering Conference, 24–28 September, DETC2005-84787, Long Beach, CA (2005)
26. Wang, C.C.: Nonlinear dynamic behavior and bifurcation analysis of a rigid rotor supported by a relatively short externally pressurized porous gas journal bearing system. Acta Mech. **183**(1–2), 41–60 (2006)
27. Yamamoto, T., Ishida, Y.: Linear and Nonlinear Rotordynamics. Wiley, New York (2001)